Journal of Applied Physics ARTICLE scitation.org/journal/jap

Electronic and optical properties of highly boron-doped epitaxial Ge/AlAs(001) heterostructures

Cite as: J. Appl. Phys. **127**, 075702 (2020); doi: 10.1063/1.5130567
Submitted: 4 October 2019 · Accepted: 2 February 2020 ·
Published Online: 18 February 2020

Michael B. Clavel,[1] Jheng-Sin Liu,[1] Michael A. Meeker,[2] Giti A. Khodaparast,[2] Yuantao Xie,[2] Jean J. Heremans,[2] Shuvodip Bhattacharya,[1] and Mantu K. Hudait[1,a)]

AFFILIATIONS

[1]Advanced Devices & Sustainable Energy Laboratory (ADSEL), Bradley Department of Electrical and Computer Engineering, Virginia Tech, Blacksburg, Virginia 24061, USA
[2]Department of Physics, Virginia Tech, Blacksburg, Virginia 24061, USA

[a)]**Author to whom correspondence should be addressed:** mantu.hudait@vt.edu

ABSTRACT

The impact of elemental boron (B) doping on the structural, optical, and magnetotransport properties of epitaxial Ge/AlAs/GaAs(001) heterostructures, grown by solid-source molecular beam epitaxy, was comprehensively investigated. Cross-sectional transmission electron microscopy analysis revealed atomically abrupt Ge:B/AlAs and AlAs/GaAs heterointerfaces and a lack of observable long-range defect formation or B segregation in the epitaxial Ge:B layer. Spectral broadening observed in the measured temperature-dependent photoluminescence spectra suggested valence band mixing during recombination, implying a splitting of the valence band heavy- and light-hole degeneracy due to residual strain resulting from substitutional B incorporation in the Ge epilayer. Temperature-dependent magnetotransport analysis of the B-doped Ge thin films exhibited the tell-tale signature of antilocalization, indicating observable spin–orbit interaction in the Ge:B system. Moreover, the temperature- and magnetic field-dependent magnetotransport results indicate the presence of single-carrier, *p*-type conduction in the Ge:B film, further affirming the successful incorporation and activation of B at a high concentration ($\sim 4 \times 10^{19}$ cm^{-3}) and elimination of parallel conduction via the large-bandgap AlAs buffer. Together, these results provide insights into the effects of heavy doping (via elemental solid-source doping) on Ge-based heterostructures and their feasibility in future electronic and photonic applications.

I. INTRODUCTION

Highly doped Ge, $Ge_{1-x}Sn_x$, and $Si_{1-x}Ge_x$ thin films have attracted considerable research interest over the past decade due to their numerous applications in (i) complementary metal-oxide-semiconductor (CMOS) technologies beyond the 10 nm technology node;[1–3] (ii) the monolithic integration of photonic and optoelectronic devices with CMOS integrated circuits;[4–7] and (iii) spintronic devices for use in quantum computing.[8,9] Moreover, as the heterogeneous integration of Ge-based materials on multiple substrates increasingly garners interest due to its applicability in high-density integration,[10,11] understanding the optical and magnetotransport behavior of complex, highly doped Ge-based heterostructures has become essential. Whereas previous investigations[12–20] have largely focused on (i) the structural implications of doping Ge-based films at or above their solid solubility limit (5×10^{19} cm^{-3}–1×10^{20} cm^{-3})[3] or (ii) the optical and magnetotransport behavior of bulk or bulklike Ge materials,[21–25] little effort has been devoted toward elucidating the impact that high dopant concentrations have on the temperature-dependent optical and magnetotransport properties of highly doped Ge-based heterostructures, crucial for understanding the feasibility of these heterostructures in future electronic and photonic devices.

One such heterostructure that has recently shown promise for both electronic[26–29] and photonic[30–33] applications is the (AlAs/) Ge/AlAs heterostructure, wherein the AlAs layer(s) acts to confine carrier transport or recombination to the Ge layer.[28] Notably,

carrier confinement and the elimination of parallel conduction from underlying buffer layers has been demonstrated to reduce quantum well field-effect transistor reverse-bias leakage current by 10^3 A/μm, simultaneously improving device subthreshold slope, both key performance metrics for the prospective adoption of Ge-based CMOS logic.[34] Moreover, from a growth perspective, the bottom AlAs layer serves as an epitaxial (potentially metamorphic) buffer, as well as a means to minimize both atomic interdiffusion and crystallographic defect propagation into the electronically/optically active region.[32,35] Significantly, minimizing the cross diffusion of atomic species at the heterointerface is imperative, as previous work has demonstrated degraded photoluminescence (PL) intensity and spectral broadening resulting from Ge and As diffusion in as-grown GaAs/Ge heterostructures absent of an, for example, AlAs barrier layer.[32] Consequently, this work investigates the influence of high, active dopant concentrations on the structural properties, and temperature-dependent optical and magnetotransport behavior of boron-doped (B-doped) Ge/AlAs heterostructures grown via dual-chamber molecular beam epitaxy (MBE) and integrated into GaAs(001) substrates. Boron has been selected as a *p*-type dopant due to its ability to exhibit both uniform and abrupt dopant profiles while simultaneously maintaining $\geq 10^{19}$ cm^{-3} active dopant concentrations.[36] Such dopant behavior is critically important in emerging electronic devices, such as tunnel field-effect transistors, wherein the dopant abruptness, uniformity, and concentration at the source/channel tunneling heterointerface determine the interfacial electric field magnitude, and thereby the tunneling probability and associated tunneling (i.e., device) current.[37] Moreover, utilizing GaAs as a starting platform, such heterostructures can subsequently be metamorphically grown on, e.g., Si substrates, thereby enabling economically feasible monolithic integration of Ge-based electronic and optoelectronic devices in the future.

II. EXPERIMENT

For this study, the B-doped Ge/AlAs/GaAs(001) heterostructures were grown using solid-source MBE utilizing separate group IV and III–V growth chambers connected via an ultrahigh vacuum transfer chamber. The initiating (001)GaAs substrates were desorbed of residual surface oxides at 750 °C under an As_2 overpressure of $\sim 10^5$ Torr, after which, a 250 nm GaAs homoepitaxial buffer was subsequently grown. Following homoepitaxial GaAs growth, the 170 nm AlAs high-bandgap buffer was grown, after which, the substrate was gradually (5 °C/min) cooled to 150 °C prior to being transferred to the group IV growth chamber for growth of the 290 nm B-doped Ge epilayer. Both AlAs and GaAs epitaxy utilized a growth temperature of 650 °C and growth rates of 0.25 μm/h and 0.5 μm/h, respectively. Conversely, a low Ge growth rate of ~0.07 Å/s and growth temperature of 400 °C were selected in order to minimize interfacial atomic diffusion at the Ge/AlAs heterointerface during Ge epitaxy. *In situ* high-energy electron diffraction (RHEED) was used to evaluate the surface reconstruction at all stages of growth, thereby ensuring optimal deposition conditions to maintain layer-by-layer (i.e., Frank–van der Merwe) epitaxy. We note that all temperatures discussed in this work refer to the thermocouple temperature.

To determine the impact of B doping on the structural and heterointerfacial properties of the as-grown Ge/AlAs/GaAs(001) heterostructures (Fig. 1), cross-sectional transmission electron microscopy (X-TEM) analysis was performed utilizing a JEOL 2100 TEM. The required electron transport foils were prepared via mechanical grinding, dimpling, and low-temperature Ar^+ ion beam milling of representative heterostructure cross sections. Additionally, the effect of B doping on the optical properties of the Ge:B/AlAs/GaAs(001) heterostructures was investigated via temperature-dependent photoluminescence (PL) spectroscopy from 77 K to 298 K. A Ti:sapphire laser ($\lambda = 700$ nm) with a repetition rate of 80 MHz, a pulse duration of ~140 fs, and a spot size of ~200 μm was used as the optical excitation source. The emitted light was passed through a 0.55 m focal length spectrometer and collected by an InGaAs detector using a standard lock-in detection scheme with a chopper frequency of ~331 Hz. Likewise, the magnetotransport properties were studied as a function of temperature ($4\ \text{K} \leq T \leq 293\ \text{K}$) and perpendicularly applied magnetic field ($B \leq \pm 1.4$ T) in order to determine the carrier type, density, and mobility, as well as to ascertain the presence of single- or multi-carrier conduction within the as-grown heterostructures. To this end, ~3×3 mm^2 samples were prepared in the van der Pauw configuration utilizing a 10 nm Ti/10 nm Pt/100 nm Au contacting scheme deposited via a Kurt J. Lesker PVD250 physical vapor deposition (PVD) chamber subsequent to a 60 s dilute hydrofluoric acid clean to remove residual native Ge oxides.

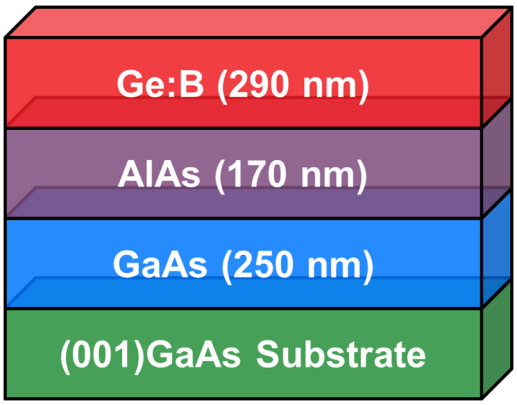

FIG. 1. Cross-sectional schematic of the Ge:B/AlAs/GaAs(001) heterostructure investigated in this work.

III. RESULTS AND DISCUSSION

As hitherto discussed, the structural evaluation of the as-grown Ge:B/AlAs heterostructures was performed utilizing TEM in order to reveal their microstructural and heterointerface properties, including (i) defect formation (if any) and (ii) heterointerface abruptness. Correspondingly, Fig. 2 shows the low- and high-magnification TEM micrographs recorded from a representative cross section of a Ge:B/AlAs/GaAs(001) heterostructure. One can find from Fig. 2(a) that no observable long-range defects were introduced by the elemental B doping of the Ge epilayer; however, ion-milling damage was evidenced by the partially amorphized AlAs buffer. High-magnification

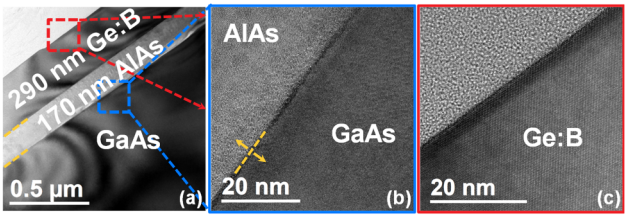

FIG. 2. (a) Low-magnification cross-sectional TEM micrograph of the Ge:B/AlAs/GaAs(001) heterostructure showing that no observable long-range defects were introduced by high concentration B doping. Representative high-magnification micrographs of the (b) AlAs/GaAs interface and (c) Ge:B surface demonstrate the heterointerfacial abruptness and lack of B segregation[38] in the Ge epilayer.

imaging of intact crystalline AlAs regions near the AlAs/GaAs heterointerface, shown in Fig. 2(b), confirmed the crystallinity of the as-grown AlAs as well as its abruptness at either interface. This is reinforced via previously reported TEM analysis of similar Ge:*uid*/AlAs/GaAs(001) heterostructures grown on GaAs(001)[26] and Si(001)[10] substrates, wherein optimal ion-milling conditions yielded TEM micrographs absent of preparation artifacts. Examination of the high-magnification micrograph of a representative region at the Ge:B surface [Fig. 2(c)] corroborates the previous conclusion that incorporation of a high concentration of B leads to neither long-range defect formation (e.g., threading dislocations, micro twinning, or stacking faults) nor surface segregation of B during growth, as previously observed during epitaxy of highly B-doped Si thin films.[38] Figure 3 (top) further reaffirms this conclusion, wherein the $20 \times 20\,\mu m^2$ atomic force microscopy (AFM) micrograph taken from a representative region of the Ge:B epilayer's surface exhibited a low RMS roughness (R_q) of 3.16 nm and a uniform surface morphology (Fig. 3, bottom). Indeed, these data are comparable to previously reported[28] surface roughness results for unintentionally doped Ge/AlAs/GaAs(001) heterostructures, revealing no statistically significant modification to the RMS surface roughness as a function of B incorporation in the epitaxial Ge layer.

Figure 4(a) presents the measured temperature-dependent PL spectra for the Ge:B/AlAs/GaAs(001) heterostructure, in which only those spectral features associated with the Ge:B epilayer were detected. As shown in Fig. 4(a), a qualitative decrease in PL spectral intensity as a function of measurement temperature was observed below 298 K. Given the excitation power used in this work (580 mW ≈ 0.461 kW/cm^2), the observed reduction in emission likely stems from inefficient scattering between L-valley electrons and available states in the Γ-valley of *p*-Ge:B. This is in contrast to the case of *n*-Ge, wherein the increased electron concentration acts to fill L-valley states (prior to optical excitation), thereby reducing the energy threshold required for momentum-conserving electron scattering into available Γ-valley states. This increase in electron state filling in *n*-type Ge materials is well understood to correspond to greatly enhanced PL intensity.[39,40] Moreover, as can be seen in Fig. 4(a), the measured direct transition spectral feature was quite broad, exhibiting a full-width at half-maximum (FWHM) value of 0.18 eV at 293 K. A similarly broad PL peak width was previously seen in highly *p*-doped Ge[41] and was attributed to a convolution of

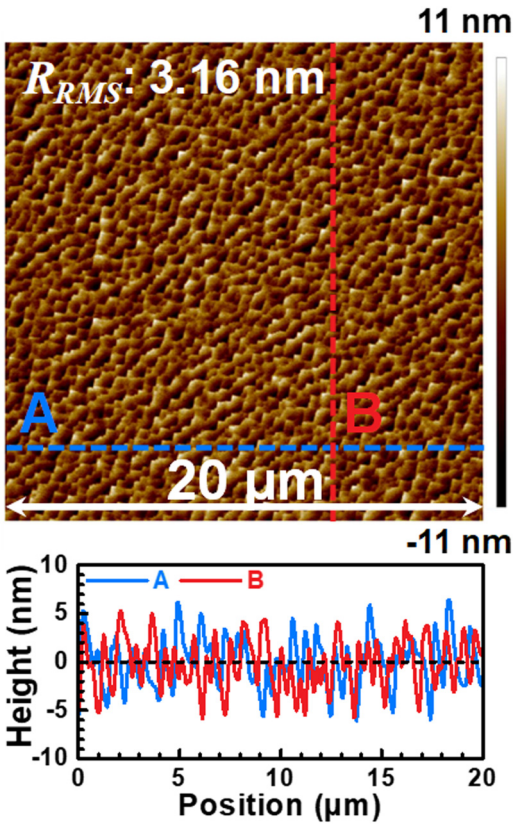

FIG. 3. (Top) $20 \times 20\,\mu m^2$ AFM micrograph of the Ge:B epilayer surface, demonstrating RMS roughness comparable to that of previously reported[28] Ge:*uid*/AlAs/GaAs(001) heterostructures. (Bottom) Orthogonal line height profiles revealing uniform surface morphology and a maximum peak-to-valley height of ∼10 nm.

the direct (and likewise, the indirect) transition with transitions resulting from carrier scattering by ionized acceptors and carrier–carrier interaction. A broadening in the PL peak width was also observed in strained *n*-Ge,[39] wherein the strain acts to split the heavy- and light-hole valence band degeneracy, thereby resulting in mixed-valence band recombination behavior. Given the large atomic covalent radius difference between Ge and B,[42] it is possible that the substitutional incorporation of B within the Ge host lattice results in a local bond length distortion of surrounding Ge–Ge bonds. If, in such a case, the strain energy imparted onto the lattice is insufficient for the nucleation of defects to occur and strain relaxation to take place,[43] then some amount of residual Ge strain could be expected. Indeed, the recent work by Clavel *et al.*[35] empirically demonstrates and theoretically describes the development of 0.29 ± 0.05% tensile strain in B-doped Ge films resulting from the physical description provided above. In light of this, it is therefore probable that both of the aforementioned spectral broadening mechanisms contribute to the observed PL peak broadening in the Ge:B/AlAs/GaAs(001) heterostructure.

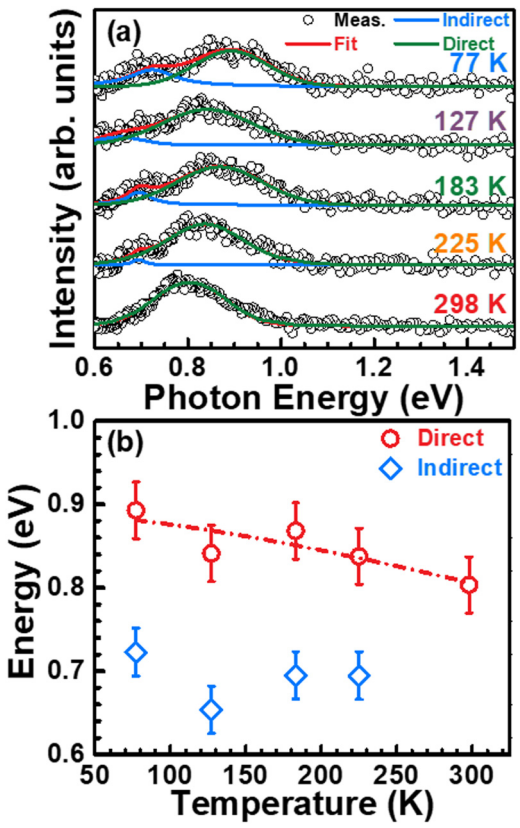

FIG. 4. (a) Temperature-dependent PL spectra recorded from the Ge:B/AlAs/GaAs(001) heterostructure. (b) Varshni fitting (dotted–dashed line) of the empirical direct and indirect transition energies (symbols; extracted using Gaussian/Lorentzian peak deconvolution) as a function of temperature.

Additionally, one can find from Fig. 4(a) that only direct recombination emission was observed in the 298 K PL spectra associated with the Ge:B epilayer. However, the position of the direct transition at 0.89 eV differs from its expected red shift as a function of increasing hole concentration[41,44] and in the presence of tensile strain.[45–47] Whereas at decreased temperatures increasing indirect emission was observed at lower photon energies, due to the InGaAs detector cutoff energy, the experimental Ge:B indirect transition was not fully resolvable. Moreover, the direct transition energy exhibited a red-blue-red shift between 183 K and 77 K, which may indicate the presence of localized states.[48] Briefly, at the lowest measurement temperatures, charge is trapped in local potential minima, from which it recombines. As the temperature is increased, localized charge can be thermalized out of the shallowest traps; however, trapped charge residing in deeper trap states will have insufficient energy to escape, thus resulting in a red shift of the peak energy. By further increasing the measurement temperature, charged trapped in the deeper trap states can also be thermalized, thereby allowing for recombination at the fundamental bandgap, resulting in a blue shift of the peak energy. Ultimately, the peak energy will shift with the bandgap at even higher temperatures, thus redshifting the peak energy once again. Taken together, these results suggest a decrease in the (hole) quasi-Fermi energy level, $E_{F,p}$, to within the Ge valence band due to the high B dopant concentration. Moreover, it has recently been shown that crystallographic defects result in trap states ~0.4–0.5 eV below the Ge valence band.[49] Consequently, a decrease in $E_{F,p}$ to within the Ge valence band could be expected to increase trap interaction should $E_{F,p}$ reside below the aforementioned trap energy level, thereby partially explaining the observed Ge:B PL emission phenomena. Finally, in order to determine the temperature dependence of the observed PL emission features, the measured direct and indirect transition energies associated with the Ge:B epilayer were fit to the Varshni equation, the results of which are presented in Table I and graphically depicted in Fig. 4(b). A comparison of the Varshni parameters highlighted in Table I with previously reported results (Table II) for bulk Ge[50,51] and thick Ge epitaxially grown on Si substrates[52,53] revealed good agreement between the data, indicating the bulklike nature of the Ge:B epilayer dominating the PL behavior of the Ge:B/AlAs heterostructure investigated herein.

Having investigated the impact of high B dopant concentration on the temperature-dependent PL properties of Ge:B/AlAs/GaAs(001) heterostructures, we now turn our attention to its effect on the magnetotransport behavior of such heterostructures. To this end, magnetotransport properties were obtained from representative B-doped Ge/AlAs/GaAs(001) heterostructure samples measured in the van der Pauw configuration from 4 K to 293 K under an applied magnetic field, B, parallel to the growth direction. Figure 5(a) depicts the measured sheet resistance, $R_{\square}(B = 0)$, as a function of temperature for the as-grown Ge:B/AlAs/GaAs(001) heterostructure, from which it can be seen that the heterostructure

TABLE I. Direct and indirect transition energies in the *p*-Ge:B/AlAs/GaAs(001) heterostructure.

	p-Ge:B	
Temperature (K)	Direct transition (eV)	Indirect transition (eV)
77	0.89	0.72
128	0.84	0.65
183	0.87	0.69
225	0.84	0.69
298	0.80	
Varshni parameters	$E_g^{\Gamma}(T) = 0.89 - \frac{5.60\times10^{-4}T^2}{(T+296)}$	

TABLE II. Comparison of the Varshni parameters found in this work with previous bulk and epitaxial Ge fitting data.

E_0 (eV)	α ($\times10_{ev}^{-4\alpha}k^{-1}$)	β (K)	Reference
0.8893	6.842	398	50
0.892	7.25	433	51
0.853	5.82	296	52
0.85	5.82	296	53
0.89	5.60	296	This work

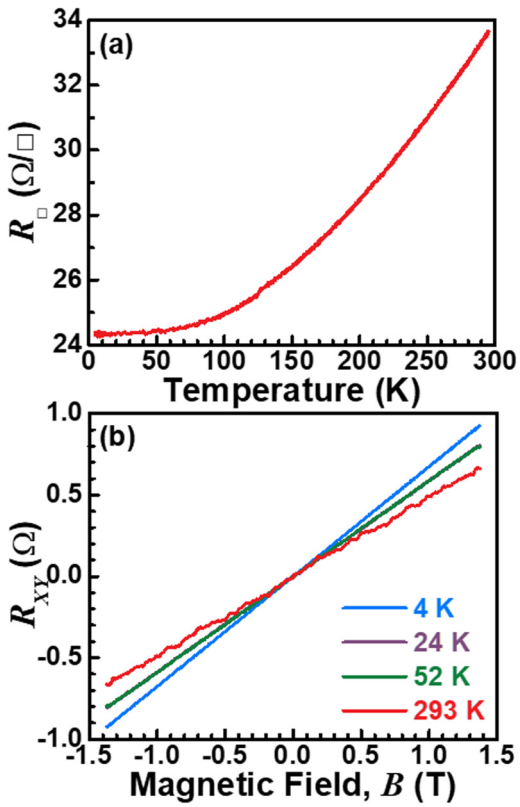

FIG. 5. (a) Sheet resistance, $R_\square$, as a function of temperature for the Ge:B/AlAs/GaAs(001) heterostructure. (b) Hall resistance, R_{XY}, as a function of magnetic field for the same, measured from 4 K to 52 K, and 293 K.

exhibited metallic conductivity behavior. To characterize the carrier type(s) and their densities (denoted N_h for p-type), the Hall resistance, R_{XY}, as a function of temperature (4.0 K to 52 K, and 293 K) and applied B ($\lesssim\pm1.4$ T), was measured, as shown in Fig. 5(b). One can find from Fig. 5(b) that R_{XY} exhibited a linear relationship with respect to B (up to ±1.4 T) for the measured temperature range, indicating that single-carrier conduction dominates the observed transport behavior. Based on previous analysis of similar, unintentionally doped n-Ge/AlAs/GaAs(001) heterostructures, in which the heterointerfacial energy band structure confines conduction to within the Ge epilayer,[28] it can be posited that the presently observed single-carrier conduction is likewise confined to the Ge:B epilayer. Indeed, this supposition has been reaffirmed by recent investigations detailing the theoretical and experimental electronic structure at the Ge:B/AlAs heterointerface, revealing a type-1, straddling gap heterojunction.[35] Thus, when considered in tandem, these data conclusively demonstrate carrier confinement to within the epitaxial Ge:B. By fitting the measured magnetotransport data shown in Fig. 5, the carrier type and its associated density were determined for each measurement temperature, as summarized in Table III. As shown in Table III, the Ge:B epilayer was found to be p-type, noting that the sign of the slope as displayed in Fig. 5 is arbitrary due to its dependence on

TABLE III. Summary of the carrier properties in the Ge:B/AlAs/GaAs(001) heterostructure.

Temperature (K)	Sheet resistance (Ω/□)	Hole density (10^{19} cm^{-3})	Hole mobility (cm^2/V s)
4.0	24.3	3.19	277.8
25	24.4	3.67	241.0
52	24.5	3.66	240.0
293	33.4	4.41	146.0

the contact configuration used in the van der Pauw measurements. As highlighted in Table III, at $T = 4.0$ K, it was found that $N_h = 3.19 \times 10^{19}$ cm^{-3} and $R_\square = 24.3$ Ω/□, as extracted from the slope of R_{XY} vs B, wherein the extracted hole mobility, μ_h, was found to be 277.8 cm^2/V s. As the temperature was increased, N_h was found to increase (increased dopant ionization), whereas μ_h conversely decreased due to enhanced acoustic and optical-phonon scattering at elevated temperatures. Such behavior is characteristic of degenerately doped semiconductors, thereby yielding metallic properties.

Figure 6 shows the measured magnetoresistance (MR), $R_\square(B)$, as a function of applied B ($\lesssim\pm1.4$ T) and temperature (4.0–52 K) for the Ge:B/AlAs/GaAs(001) heterostructure. As can be seen in Fig. 6, the measured MR is smooth for $T \gtrsim 24$ K. However, at $T = 4$ K, the Ge:B epilayer exhibited a sharp positive MR around $B \approx 0$, manifesting as an abrupt "dip" in the MR data about $B = 0$. Such MR appearing characteristically at low temperature is associated with localization phenomena in disordered systems, originating in a quantum correction to the conductivity as a result of quantum interference between two partial carrier waves propagating on diffusive time-reversed paths.[54–57] The distribution of closed paths of variable path lengths is formed by scattering from impurities.[57] Under an applied B, the quantum interference is modified, leading to a characteristic MR. In the presence of spin–orbit interactions, the spin part of the partial waves modify the quantum interference,

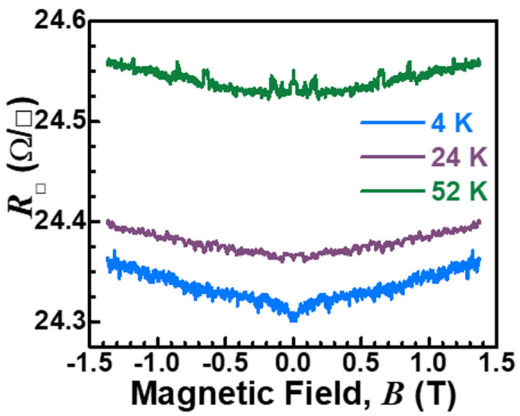

FIG. 6. Magnetoresistance (MR), $R_\square(B)$, as a function of magnetic field, B, for the Ge:B/AlAs/GaAs(001) heterostructure, measured from 4.0 K to 52 K. The signature of antilocalization (sharp positive MR) can be observed in the $B \approx 0$ MR data at $T = 4.0$ K, implying the presence of spin–orbit interaction.

leading to the phenomenon of antilocalization,[54–58] with a characteristically sharp positive MR at low B. This sharp positive MR at low B and at low temperatures has long been used to identify the presence of spin–orbit interactions.[54,57–59] The MR data collected at $T = 24$ K and $T = 52$ K, which did not exhibit an abrupt "dip" in MR at $B \approx 0$, have been included in Fig. 6 to contrast with the MR data measured at $T = 4.0$ K. As shown in Fig. 6, the MR data for $T = 24$ K and $T = 52$ K revealed a gentle parabolic positive magnetoresistance background that persisted at higher temperatures, underscoring its classical origin, whereas antilocalization is a correction due to quantum mechanical coherence and is present only at low temperatures. As such, the difference between the $T = 4.0$ K MR data and, e.g., the MR observed at $T = 24$ K is attributable to antilocalization. Furthermore, the gentle parabolic positive magnetoresistance background present at all measurement temperatures likely originates in classical geometrical magnetoresistance, as multicarrier magnetoresistance is unlikely given the single-carrier nature of the observed transport behavior. It can, therefore, be deduced that magnetotransport at $T = 4.0$ K in the Ge:B epilayer exhibited the antilocalization characteristic of spin–orbit interactions.

The relative strength of the spin–orbit interaction can be explained in light of the valence band properties. Briefly, spin–orbit interaction in semiconductor valence bands was reviewed in Ref. 59, studied theoretically,[60–62] and investigated experimentally in Ge hole systems.[63–65] These prior theoretical and experimental studies concluded that spin–orbit interaction is relatively stronger for holes in the valence band than for electrons in the conduction band (partially an effect of the effective spin 3/2 of holes in the valence bands as compared to spin 1/2 for electrons in the conduction bands).[59,66] The depth of the near-zero B "dip" in Fig. 6 (leading to the sharp positive MR observed at $T = 4.0$ K) resembles previous results[64,65] exhibiting the MR characteristic of antilocalization. Yet, it cannot necessarily be concluded that the spin–orbit interaction experienced by the holes in the Ge:B epilayer is strong, as even moderate spin–orbit interaction is detectable by antilocalization.[54] Additionally, any band splitting due to spin–orbit interaction may be commensurably moderate and may, therefore, not have had a readily detectable effect on the measured PL data. It should also be noted that the spin–orbit interaction requires a spatial symmetry breaking.[57,59,66] Given that Ge has cubic crystal symmetry, such spatial symmetry breaking must originate from a heterostructural effective electric field experienced by the carriers, here provided by the effective potential profile confining holes to the thin Ge:B epilayer.[34] The resulting effective electric field leads to structural inversion asymmetry, producing a Rashba spin–orbit interaction.[57,59,66] The magnetotransport properties are thus consistent with hole confinement and conduction in the Ge:B epilayer, with the existence of a sole carrier type having been observed. The conclusions from the magnetotransport studies are further supported by the close correspondence between the mobilities reported in this work with well-established mobility-carrier concentration trends in bulk, p-type Ge.[67]

IV. CONCLUSIONS

In summary, the impact of B doping on the optical and magnetotransport properties of epitaxial Ge/AlAs/GaAs(001) heterostructures has been systematically investigated. Demonstration of the successful growth of highly solid-source-doped Ge:B/AlAs/GaAs(001) heterostructures was validated via low- and high-magnification cross-sectional TEM analysis, indicating no observable dopant segregation or long-range defection formation as a function of substitutional B incorporation. Temperature-dependent PL analysis revealed a reduced efficiency in L-valley carrier excitation (and subsequent scattering into the Γ-valley) that limited optical recombination in the Ge:B material system. Moreover, broadening of the PL emission spectra from the Ge:B epilayer indicated mixed valence band recombination, suggesting the presence of residual strain in the Ge:B thin film due to localized Ge–Ge bond distortions introduced by substitutional B dopants. Finally, the magnetotransport behavior of the B-doped Ge/AlAs/GaAs(001) heterostructure, measured from 4 K to 52 K under $B \leq \pm 1.4$ T, revealed characteristic antilocalization phenomena, indicating the presence of spin–orbit interactions. Such a spin–orbit interaction is known to prominently manifest in valence band carrier transport, signifying confinement of hole conduction to the epitaxial Ge:B layer and an effective suppression of parallel conduction by the underlying AlAs high-bandgap buffer.

ACKNOWLEDGMENTS

M.B.C. acknowledges partial support from the National Science Foundation (NSF) under Grant No. ECCS-1507950. G.K. and M.M. acknowledge the support of the AFOSR and DURIP through Grant Nos. FA9550-17-1-0341 and FA9550-16-1-0358, respectively. The authors wish to acknowledge the Nanoscale Characterization and Fabrication Laboratory (NCFL) at the Institute for Critical Technology and Applied Science (ICTAS) and the Virginia Tech Nanofabrication facilities for assistance in materials characterization.

REFERENCES

[1]Q. C. Ouyang, M. Yang, J. Holt, S. Panda, H. Chen, H. Utomo, M. Fischetti, N. Rovedo, J. Li, N. Klymko, H. Wildman, T. Kanarsky, G. Costrini, D. M. Fried, A. Bryant, J. A. Ott, M. Ieong, and C. Y. Sung, "Investigation of CMOS devices with embedded SiGe source/drain on hybrid orientation substrates," in *Digest of Technical Papers 2005 Symposium on VLSI Technology* (IEEE, 2005).
[2]H. Yu, M. Schaekers, E. Rosseel, A. Peter, K. Hollar, F. A. Khaja, W. Aderhold, L. Date, A. J. Mayur, J. G. Lee, K. M. Shin, B. Douhard, S. A. Chew, S. Demuynck, S. Kubicek, D. Kim, A. Mocuta, K. Barla, N. Horiguchi, N. Collaert, A. V. Y. Thean, and K. De Meyer, "Ultralow-resistivity CMOS contact scheme with pre-contact amorphization plus Ti (germano-)silicidation," in *IEEE Symposium on VLSI Technology* (IEEE, 2016).
[3]J. Borland, Y. J. Lee, S. S. Chuang, T. Y. Tseng, C. W. Liu, K. Huet, G. Goodman, and J. Marino, "Solid solubility limited dopant activation of group III dopants (B, Ga & In) in Ge targeting sub-7 nm node low p+ contact resistance," in *17th International Workshop on Junction Technology* (IEEE, 2017).
[4]J. E. Roth, O. Fidaner, R. K. Schaevitz, Y. H. Kuo, T. I. Kamins, J. S. Harris, and D. A. B. Miller, Opt. Express **15**, 5851 (2007).
[5]M. Oehme, M. Gollhofer, D. Widmann, M. Schmid, M. Kaschel, E. Kasper, and J. Schulze, Opt. Express **21**, 2206 (2013).
[6]E. Kasper, M. Oehme, T. Arguirov, J. Werner, M. Kittler, and J. Schulze, Adv. OptoElectron. **2012**, 1 (2012).
[7]K. Gallacher, P. Velha, D. J. Paul, S. Cecchi, J. Frigerio, D. Chrastina, and G. Isella, Appl. Phys. Lett. **101**, 211101 (2012).
[8]P. J. Newton, J. Llandro, R. Mansell, S. N. Holmes, C. Morrison, J. Foronda, M. Myronov, D. R. Leadley, and C. H. W. Barnes, Appl. Phys. Lett. **106**, 172102 (2015).

[9]Y. Zhou, W. Han, L. T. Chang, F. Xiu, M. Wang, M. Oehme, I. A. Fischer, J. Schulze, R. K. Kawakami, and K. L. Wang, Phys. Rev. B **84**, 125323 (2011).
[10]P. D. Nguyen, M. B. Clavel, P. S. Goley, J. S. Liu, N. P. Allen, L. J. Guido, and M. K. Hudait, IEEE J. Electron Devices Soc. **3**, 341 (2015).
[11]M. K. Hudait, M. Clavel, P. Goley, N. Jain, and Y. Zhu, Sci. Rep. **4**, 6964 (2015).
[12]J. Aubin, J. M. Hartmann, M. Veillerot, Z. Essa, and B. Sermage, Semicond. Sci. Technol. **30**, 115006 (2015).
[13]S. Uppal, A. F. W. Willoughby, J. M. Bonar, A. G. R. Evans, N. E. B. Cowern, R. Morris, and M. G. Dowsett, J. Appl. Phys. **90**, 4293 (2001).
[14]T. H. Chang, C. Chang, Y. H. Chu, C. C. Lee, J. Y. Chang, I. C. Chen, and T. Li, Thin Solid Films **551**, 53 (2014).
[15]B. Han, Y. Shimizu, J. Wipakorn, K. Nishibe, Y. Tu, K. Inoue, N. Fukata, and Y. Nagai, Nanoscale **8**, 19811 (2016).
[16]Y. Bogumilowicz and J. M. Hartmann, Thin Solid Films **557**, 4 (2014).
[17]W. C. Kuo, M. J. Lee, M. L. Wu, C. C. Lee, I. Y. Tsao, and J. Y. Chang, Solid State Electron. **130**, 41 (2017).
[18]A. Satta, E. Simoen, T. Clarysse, T. Janssens, A. Benedetti, B. De Jaeger, M. Meuris, and W. Vandervorst, Appl. Phys. Lett. **87**, 172109 (2005).
[19]L. Hutin, S. Koffel, C. Le Royer, L. Clavelier, P. Scheiblin, V. Mazzocchi, and S. Deleonibus, Mater. Sci. Semicond. Process. **11**, 267 (2008).
[20]W. S. Jung, J. H. Nam, A. Pal, J. H. Lee, Y. Na, Y. Kim, J. H. Lee, and K. C. Saraswat, IEEE Electron Device Lett. **36**, 297 (2015).
[21]W. G. Spitzer, F. A. Trumbore, and R. A. Logan, J. Appl. Phys. **32**, 1822 (1961).
[22]P. J. Dean, J. R. Haynes, and W. F. Flood, Phys. Rev. **161**, 711 (1967).
[23]L. Viña and M. Cardona, Phys. Rev. B **34**, 2586 (1986).
[24]R. R. Lieten, K. Bustillo, T. Smets, E. Simoen, J. W. Ager, E. E. Haller, and J. P. Locquet, Phys. Rev. B **86**, 035204 (2012).
[25]R. Camacho-Aguilera, Z. Han, Y. Cai, L. C. Kimerling, and J. Michel, Appl. Phys. Lett. **102**, 152106 (2013).
[26]P. D. Nguyen, M. B. Clavel, J. S. Liu, and M. K. Hudait, IEEE Trans. Electron Devices **64**, 4457 (2017).
[27]P. D. Nguyen, M. B. Clavel, A. Ghosh, and M. K. Hudait, Microelectron. Eng. **199**, 80 (2018).
[28]M. K. Hudait, M. Clavel, P. Goley, Y. Xie, and J. J. Heremans, ACS Appl. Mater. Interfaces **7**, 22315 (2015).
[29]T. Maeda and H. Tanaka, J. Cryst. Growth **201-202**, 194 (1999).
[30]Y. Cai, Z. Han, X. Wang, R. E. Camacho-Aguilera, L. C. Kimerling, J. Michel, and J. Liu, IEEE J. Sel. Top. Quantum Electron **19**, 1901009 (2013).
[31]S. Cho, B. G. Park, C. Yang, S. Cheung, E. Yoon, T. I. Kamins, S. J. B. Yoo, and J. S. Harris, Opt. Express **20**, 14921 (2012).
[32]C. K. Chia, J. R. Dong, D. Z. Chi, A. Sridhara, A. S. W. Wong, M. Suryana, G. K. Dalapati, S. J. Chua, and S. J. Lee, Appl. Phys. Lett. **92**, 141905 (2008).
[33]C. K. Chia, G. K. Dalapati, Y. Chai, S. L. Lu, W. He, J. R. Dong, D. H. L. Seng, H. K. Hui, A. S. W. Wong, A. J. Y. Lau, Y. B. Cheng, D. Z. Chi, Z. Zhu, Y. C. Yeo, Z. Xu, and S. F. Yoon, J. Appl. Phys. **109**, 066106 (2011).
[34]R. Pillarisetty, B. Chu-Kung, S. Corocoran, G. Dewey, J. Kavalieros, H. Kennel, R. Kotlyar, V. Le, D. Lionberger, M. Metz, N. Mukherjee, J. Nah, W. Rachmady, M. Radosavljevic, U. Shah, S. Taft, H. Then, N. Zelick, and R. Chau, in *International Electron Devices Meeting* (IEEE, 2010), p. 150.
[35]M. B. Clavel, G. Greene-Diniz, M. Grüning, K. T. Henry, M. Kuhn, R. J. Bodnar, and M. K. Hudait, ACS Appl. Electron. Mater. **1**, 2646 (2019).
[36]V. P. Kesan, S. S. Iyer, and J. M. Cotte, J. Cryst. Growth **111**, 847 (1991).
[37]J. S. Liu, M. B. Clavel, and M. K. Hudait, IEEE Trans. Electron Devices **62**, 3223 (2015).
[38]C. P. Parry, R. A. A. Kubiak, S. M. Newstead, E. H. C. Parker, and T. E. Whall, Mater. Res. Soc. Symp. Proc. **220**, 103 (1991).
[39]X. Sun, J. Liu, L. C. Kimerling, and J. Michel, Appl. Phys. Lett. **95**, 011911 (2009).
[40]M. El Kurdi, T. Kociniewski, T. P. Ngo, J. Boulmer, D. Débarre, P. Boucaud, J. F. Damlencourt, O. Kermarrec, and D. Bensahel, Appl. Phys. Lett. **94**, 191107 (2009).
[41]J. Wagner and L. Viña, Phys. Rev. B **30**, 7030 (1984).
[42]P. Pyykkö, Phys. Rev. B **85**, 024115 (2012).
[43]R. People and J. C. Bean, Appl. Phys. Lett. **47**, 322 (1985).
[44]S. C. Jain and J. D. Roulston, Solid State Electron. **34**, 453 (1991).
[45]M. El Kurdi, H. Bertin, E. Martincic, M. de Kersauson, G. Fishman, S. Sauvage, A. Bosseboeuf, and P. Boucaud, Appl. Phys. Lett. **96**, 041909 (2010).
[46]T. H. Cheng, K. L. Peng, C. Y. Ko, C. Y. Chen, H. S. Lan, Y. R. Wu, C. W. Liu, and H. H. Tseng, Appl. Phys. Lett. **96**, 211108 (2010).
[47]Y. Ishikawa, K. Wada, J. Liu, D. D. Cannon, H. C. Luan, J. Michel, and L. C. Kimerling, J. Appl. Phys. **98**, 013501 (2005).
[48]T. R. Merritt, M. A. Meeker, B. A. Magill, G. A. Khodaparast, S. McGill, J. G. Tischler, S. G. Choi, and C. J. Palmstrøm, J. Appl. Phys. **115**, 193503 (2014).
[49]J. R. Weber, A. Janotti, P. Rinke, and C. G. Van de Walle, Appl. Phys. Lett. **91**, 142101 (2007).
[50]Y. P. Varshni, Physica **34**, 149 (1967).
[51]P. A. Dafesh and K. L. Wang, Phys. Rev. B **45**, 1712 (1992).
[52]M. Y. Ryu, T. R. Harris, Y. K. Yeo, R. T. Beeler, and J. Kouvetakis, Appl. Phys. Lett. **102**, 171908 (2013).
[53]Y. H. Kil, J. H. Yang, S. Kang, D. J. Kim, T. S. Jeong, C. J. Choi, T. S. Kim, and K. H. Shim, Mater. Sci. Semicond. Process. **21**, 58 (2014).
[54]G. Bergmann, Int. J. Mod. Phys. B **24**, 2015 (2010).
[55]R. L. Kallaher and J. J. Heremans, Phys. Rev. B **79**, 075322 (2009).
[56]R. L. Kallaher, J. J. Heremans, N. Goel, S. J. Chung, and M. B. Santos, Phys. Rev. B **81**, 075303 (2010).
[57]M. Kohda, T. Bergsten, and J. Nitta, J. Phys. Soc. Jpn. **77**, 031008 (2008).
[58]G. Bergmann, Solid State Commun. **42**, 815 (1982).
[59]W. Zawadzki and P. Pfeffer, Semicond. Sci. Technol. **19**, R1 (2004).
[60]O. Mauritz and U. Ekenberg, Phys. Rev. B **55**, 10729 (1997).
[61]N. S. Averkiev, L. E. Golub, and G. E. Pikus, J. Exp. Theor. Phys. **86**, 780 (1998).
[62]L. E. Golub and S. Pedersen, Phys. Rev. B **65**, 245311 (2002).
[63]R. Moriya, K. Sawano, Y. Hoshi, S. Masubuchi, Y. Shiraki, A. Wild, C. Neumann, G. Abstreiter, D. Bougeard, T. Koga, and T. Machida, Phys. Rev. Lett. **113**, 086601 (2014).
[64]C. Morrison, J. Foronda, P. Wiśniewski, S. D. Rhead, D. R. Leadley, and M. Myronov, Thin Solid Films **602**, 84 (2016).
[65]J. Foronda, C. Morrison, J. E. Halpin, S. D. Rhead, and M. Myronov, J. Phys. Condens. Matter **27**, 022201 (2015).
[66]R. Winkler, *Spin-Orbit Coupling Effects in Two-Dimensional Electron and Hole Systems*, Springer Tracts in Modern Physics Vol. 191 (Springer-Verlag Berlin, Heidelberg, 2003).
[67]L. E. Vorobyev, *Handbook Series on Semiconductor Parameters* (World Scientific River Edge, 1996), Vol. 1.